# Aperiodic space-time modulation for pure frequency mixing

Sajjad Taravati
*Department of Electrical Engineering, Poly-Grames Research Center, Polytechnique Montréal, Montréal, Quebec, Canada H3T 1J4*

(Received 18 December 2017; published 14 March 2018)

This paper experimentally demonstrates the effects of inharmonic photonic transition in tailored aperiodic space-time refractive index modulated media. Such effects introduce a pure frequency mixing based on the simultaneous and distinct shifts in the spatial and temporal frequencies. The medium is characterized with a periodic temporal modulation and a tailored aperiodic spatially modulated permittivity and permeability, yielding aperiodic, large and tunable photonic band gaps. Since the medium is time periodic, an infinite number of space-time mixing products are generated with a distance equal to the temporal frequency of the pump wave. However, thanks to the tailored spatial aperiodicity of the medium and associated photonic band gaps, transition to unwanted space-time mixing products is prohibited. Interesting features include tunability of the operation frequencies of the mixer via space-time modulation parameters, high isolation, linear response, and possibility of conversion gain due to the transfer of energy and momentum of the space-time modulation to the input wave. We derive the analytical solution for such mixer with aperiodic space-modulated permittivity and permeability and periodic time modulation, and then provide the synthesis procedure which takes into account the effects of space-time modulation inhomogeneity. Finally, to see the effect of the tailoring of space modulation, we compare the experimental results of the aperiodic space-time modulated pure mixer with those of the conventional periodic uniform space-time modulated medium.

DOI: 10.1103/PhysRevB.97.115131

## I. INTRODUCTION

Frequency mixing of electromagnetic waves represents a vital functionality for a great number of applications ranging from radio astronomy and military radars to biological sensing systems. This is conventionally achieved by nonlinear components, e.g., Schottky diodes, GaAs field-effect transistors, and complementary metal-oxide semiconductor transistors [1–3], whereas nonlinear response of the component results in generation of an infinite number of mixing products. Theoretically, the frequency components generated by a single diode read $\omega_O = m\omega_0 \pm n\omega_{LO}$, where $m$ and $n$ are all integers, $\omega_0$ and $\omega_{LO}$ are temporal frequencies of the two input waves, and $\omega_O$ is the temporal frequency of the output wave. However, we only desire one output frequency, e.g., $n = 1$ and $m = 1$, whereas the existence of all other harmonic terms creates significant problems, and elimination of these distortion products is the key aim in mixer technology. Over the past few decades, many efforts have been made to realize harmonic-rejection mixers; however, conventional mixers, even in their most ideal realizations, still suffer from undesirable mixing products. Switching mixers, subsampling mixers, and microwave photonic mixers suffer from the same problem [4–6].

Space-time refractive-index modulation may be represented as an alternative approach for achieving mixing products of two frequencies [7–13]. The space-time modulation technique exhibits high isolation and compatibility with circuit technology and integrated optical networks. It has been recently utilized for the realization of a new class of microwave and optical isolators [10,11,14–19], circulators [20,21], nonreciprocal metasurfaces [22–25], and nonreciprocal integrated systems [26–28]. Up to now, all reported space-time modulations are periodic in both space and time. However, periodic space-time modulation provides the required energy and momentum for transition from fundamental temporal frequency $\omega_0$ to an infinite number of space-time frequency harmonics, i.e., $\omega_O = \omega_0 \pm n\omega_p$ with $\omega_p$ being the pump wave frequency [8,11,13,29]. The common way to experimentally realize the space-time modulation is to use a pump wave that spatiotemporally modulates an array of distributed varactors on a transmission line [26–28,30]. However, in experiment, the input wave may also modulate the varactors, and thus, both the pump wave and the input wave will contribute harmonics, so that $\omega_O = m\omega_0 \pm n\omega_p$ [11,27,30]. Periodically, space-time modulated leaky-wave systems may exhibit pure leaky-wave frequency mixing and radiation, where the leaky-wave radiation of unwanted harmonics is prohibited by the light cone [26–28,31].

This study introduces a general technique for pure frequency mixing in space-time modulated media, where harmonic photonic transitions in temporally periodic systems are prohibited by *tailored* photonic band gaps introduced by the engineered spatial aperiodicity of the structure. In contrast to conventional periodic uniform space-time modulated media, here the medium is *aperiodic* in space and therefore exhibits an aperiodic dispersion diagram and photonic band gaps tailored in a way to provide photonic band gaps at undesired space-time mixing products, and hence, introduces a pure frequency mixing. It should be noted that such a time-periodic system still generates all the unwanted harmonics, whereas due to the existence of tailored band gaps the progressive growth of these unwanted space-time mixing products is prohibited. The proposed mixer inherits the linearity property of space-time modulated media. In addition, the frequency bands of the mixer may be tuned via space-time modulation parameters. The proposed mixer takes advantage of the aperiodic spatially varying structures which are capable of providing

 

a variety of electromagnetic responses that are unattainable by uniform structures. Such structures have introduced a variety of enhanced efficiency electromagnetic systems, such as, for instance, broadband and multiband power dividers [32,33], very large scale integrated interconnection structures [34,35], matching circuits of multiplexers [36], directional filters [37], phase shifters and group delay engineering [38–41], impedance transformers [42], and miniaturized and broadband rat race and branch-line couplers [43–45].

## II. APERIODIC SPACE-TIME MODULATION

Consider a periodic space-time modulated medium represented by a particular periodic space-time varying permittivity $\epsilon(z,t) = \epsilon_r[1 + \delta_p \cos(\beta_p z - \omega_p t)]$ [7,8,10,11], where $\epsilon_r$ is the permittivity of medium, $\delta_p$ represents the pumping depth, and $\beta_p$ and $\omega_p$ respectively denote the spatial frequency and temporal frequency of the pump wave. Such a medium possesses a dispersion diagram as depicted in Fig. 1(a). This diagram consists of an infinite periodic set of $\beta_n/\beta_p - \omega_n/\omega_p$ straight lines, where $\beta_n = \beta_0 + n\beta_p$ and $\omega_n = \omega_0 + n\omega_p$ with $n$ being any integer. To any frequency, $\omega_0$, corresponds an infinite number of modes, each of which include an infinite number of forward and backward space-time harmonics, i.e., $(\beta_0 + n\beta_p, \omega_0 + n\omega_p)$ [8,11,29]. However, in practice only one of these harmonics may be required and all others should be filtered out. This represents a waste of energy and design and fabrication complexities. Different from conventional mixers, in a periodic space-time modulated medium, the input wave at $\omega_0$, theoretically, will not space-time modulate the structure, and thus will not contribute to harmonic generation. In experiment, however, due to the implementation restrictions, the input wave may also space-time modulate the structure [11,27,30], and hence contribute to space-time harmonic generation, yielding a transition from $(\beta_0, \omega_0)$ to $[k\beta_0 + n\beta_p, k\omega_0 + n\omega_p]$, with $k,n$ all being integers. As a consequence, such a periodic space-time modulated medium practically introduces the same mixing products as conventional mixers. Furthermore, as the space-time modulation is experimentally demonstrated by a pump wave at $\omega_p$ that spatiotemporally modulates an array of subwavelength spaced varactors [11,19,27,28], the harmonics of the pump wave $n\omega_p$ may show up at the output. The output spectrum of a particular periodic space-time modulated medium is shown in the inset of Fig. 1(a).

Here, we consider the case of an *aperiodic* space-time modulated medium with thickness $L$, spatially aperiodic and temporally periodic permittivity as

$$\epsilon(z,t;\omega) = \epsilon_0 \epsilon_{ap}(z;\omega)[1 + \delta_p \cos(\beta_{p,ap}(z;\omega)z - \omega_p t)], \quad (1a)$$

and spatially aperiodic permeability

$$\mu(z;\omega) = \mu_0 \mu_{ap}(z;\omega), \quad (1b)$$

where $\epsilon_{ap}(z;\omega)$ and $\mu_{ap}(z;\omega)$ are aperiodic functions of space and frequency, and $\epsilon_0$ and $\mu_0$ respectively represent the permittivity and permeability of vacuum so that $\sqrt{\epsilon_0\mu_0} = 1/c$, with $c$ being the speed of light in vacuum. In (1), $\delta_p$ represents the pumping depth, and $\beta_{p,ap}(z)$ and $\omega_p$ respectively denote the spatial frequency and temporal frequency of the pump wave. The medium assumes an average spatially variant phase velocity $v_{ap}(z;\omega) = c/\sqrt{\epsilon_{ap}(z;\omega)\mu_{ap}(z;\omega)}$, where $c$ is the speed of light in vacuum, and hence the pump wave reads with an aperiodic space-dependent spatial frequency of $\beta_{p,ap}(z;\omega) = \omega_p/v_{ap}(z;\omega)$, where the subscript "p" in $\beta_{p,ap}$ and $\omega_p$ refers to "pumping" and subscript "ap" in $\beta_{p,ap}$ and $v_{ap}$ highlights that they are "aperiodic" functions of $z$.

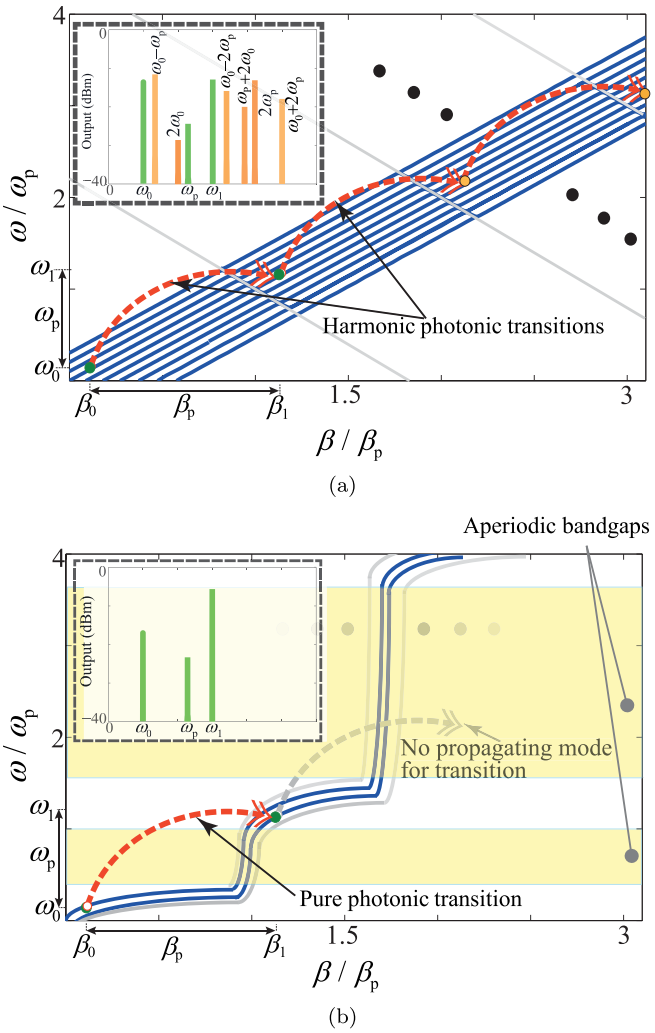


FIG. 1. Frequency generation based on photonic transitions in space-time modulated media. (a) Harmonic transitions in a periodic space-time modulated medium leads to the generation of an infinite number of space-time harmonics [8,11,29]. A particular output spectrum of such system is shown in the inset [11]. (b) Pure transition from $\omega_0$ to $\omega_1 = \omega_0 + \omega_p$ in an aperiodic space-time modulated medium (spatially aperiodic and temporally periodic) with spatially aperiodic permittivity and permeability in (1), exhibiting aperiodic photonic band gaps. The inset shows a particular output spectrum of aperiodic space-time modulated medium, where all undesired mixing products are suppressed.

Figure 1(b) plots the qualitative dispersion diagram of this aperiodic space-time modulated medium. It was shown in [11] that, in a periodic space-time medium, strong transition of energy and momentum occurs from the fundamental to the space-time harmonics, where propagation of the wave through the structure yields a *progressive* increase of the power of the space-time harmonics. As the proposed space-time modulated mixer with the constitutive parameters in (1) is still

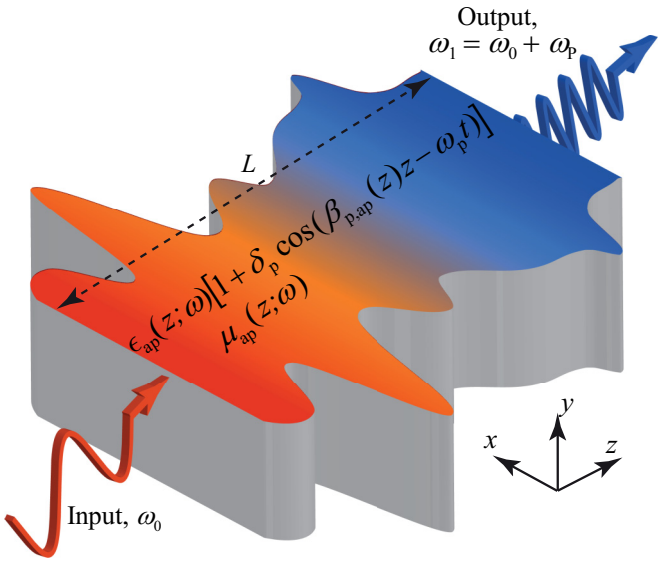


FIG. 2. Generic representation of the spatially aperiodic space-time modulated mixer with the space-time varying constitutive parameters in (1), yielding a pure frequency transition from $(\beta_0,\omega_0)$ to $(\beta_1,\omega_1)$.

time periodic, time harmonics occur at $\omega_0 + n\omega_p$. However, thanks to the tailored spatial aperiodicity of the structure, except $\omega_0$ and $\omega_1$, other undesired time harmonics lie in the band gap of the structure. Hence, they will not progressively grow up, but rather propagate as weak waves through the structure. In contrast to the periodic space-time modulation, aperiodic space-time modulation exhibits aperiodic photonic band gaps, where $\partial\beta/\partial\omega = 0$, yielding an inharmonic and distinct photonic transition, e.g., from $(\beta_0,\omega_0)$ to $(\beta_1 = \beta_0 + \beta_p,\omega_1 = \omega_0 + \omega_p)$. As a result, harmonic photonic transitions to space-time harmonics are prohibited. In addition, such medium suppresses all undesired harmonics of the input wave and the pump wave, e.g., $2\omega_0 + \omega_p$, yielding a pure frequency transition from $\omega_0$ to $\omega_1$. A qualitative output spectrum of such aperiodic space-time modulated medium is shown in the inset of Fig. 1(b) which shows suppression of undesired space-time frequency components.

The term "photonic band gap" has been introduced in the photonics field, considering the similarities between the stop-band performance of optical periodic structures, e.g., photonic crystals, and solid-state electronic band gaps. Hence, stop bands are called band gaps and periodic structures are called photonic band-gap structures [46,47]. The photonic band gap represents a forbidden energy range, where the wave behaving photons cannot be transmitted through the structure. However, aperiodic structures exhibit aperiodic stop bands which may be called aperiodic photonic band gaps [48,49].

Figure 2 shows a generic schematic of the aperiodic space-time modulated mixer possessing the qualitative dispersion diagram in Fig. 1(b). Such a spatially aperiodic structure assumes a time-periodic modulation, with $TM_x$ or $E_x$ polarization for the electromagnetic fields. Since the medium is periodic in time, the electric and magnetic fields inside it may be generally represented by the time Bloch-Floquet expansion as

$$\mathbf{E}(z,t;\omega_n) = \hat{\mathbf{x}} \sum_{n=-N}^{N} E_n(z;\omega_n) e^{-i\omega_n t}, \tag{2a}$$

$$\mathbf{H}(z,t;\omega_n) = \hat{\mathbf{y}} \sum_{n=-N}^{N} H_n(z;\omega_n) e^{-i\omega_n t}, \tag{2b}$$

where $\omega_n = \omega_0 + n\omega_p$ and $N \to \infty$. The input wave at $\omega_0$ is injected into the aperiodic space-time modulated medium in Fig. 2, and then propagates inside the medium in the $+z$ direction and experiences a photonic transition to $\omega_n = \omega_0 + n\omega_p$. However, it will be shown that with a proper spatial aperiodicity all the undesired space-time mixing products could be significantly suppressed, leading to a pure transition from $\omega_0$ to $\omega_1 = \omega_0 + \omega_p$. Such pure transition is supported by aperiodic photonic band gaps, through the aperiodicity of the medium, where all undesirable mixing products, e.g., $\omega_0 - \omega_p$ and $\omega_0 + 2\omega_p$, lie within the photonic band gaps of the medium.

## III. MIXER SYNTHESIS

Figure 3 shows a sketch of the experimental implementation of the aperiodic space-time modulated waveguide mixer with constitutive parameters in (1). This structure is composed of an array of varactors subwavelength spaced on top of an aperiodic spatially varying conductor-backed coplanar waveguide. These varactors are reverse biased at their nominal capacitive point, and will be spatiotemporally modulated using a $+z$ propagating pump wave with temporal frequency of $\omega_p$, realizing the space-time varying capacitance $C(z,t;\omega) = C_0 C_{ap}(z;\omega)\{1 + \delta_p \cos[\beta_{p,ap}(z)z - \omega_p t]\}$. This circuit emulates a medium with effective permittivity $\epsilon(z,t;\omega) = \epsilon_0\epsilon_{ap}(z;\omega)\{1 + \delta_p \cos[\beta_{p,ap}(z)z - \omega_p t]\}$ and $\mu(z;\omega) = \mu_0\mu_{ap}(z;\omega)$. The modulation depth will be controlled via the amplitude of the pump wave.

Coplanar waveguides support TEM propagation and are well suited for implementation of lumped elements since

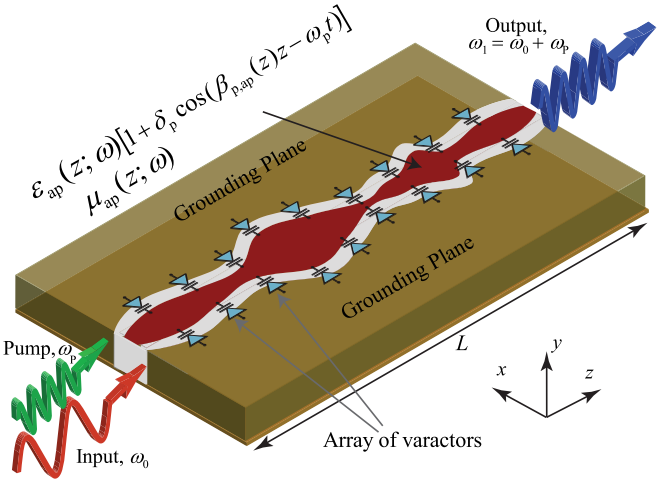


FIG. 3. Realization of an aperiodic space-time modulated mixer in Fig. 2 using an array of space-time varying varactors distributed on top of an aperiodic spatially variant conductor-backed coplanar waveguide.

ground planes are available at the top of the structure. A detailed analysis and design parameters of conductor-backed coplanar waveguides are given in [50,51].

Here we present a straightforward synthesis method for the design of the continuously spatially varying coplanar waveguides. The goal of the synthesis is to determine the spatial variation of the constitutive parameters, i.e., $\mu_{\rm ap}(z;\omega)$ and $\epsilon_{\rm ap}(z;\omega)$, providing the specified dispersion diagram. We first discretize the aperiodic spatially variant line into $Q$ deep subwavelength uniform subsections, for which closed-form formulas are available. The ray transfer matrix of each uniform subsection, with the length $l_q = L/Q \ll \lambda_{\rm min}$, may be expressed as

$$\begin{bmatrix} A_q & B_q \\ C_q & D_q \end{bmatrix} = \begin{bmatrix} \cos(\beta l) & j z_q \sin(\beta l) \\ j\dfrac{1}{z_q}\sin(\beta l) & \cos(\beta l) \end{bmatrix}. \tag{3}$$

The ray transfer matrix of the subsections hosting shunt varactors with the length $l \to 0$ reads

$$\begin{bmatrix} A_{{\rm var},q} & B_{{\rm var},q} \\ C_{{\rm var},q} & D_{{\rm var},q} \end{bmatrix} = \begin{bmatrix} 1 & 0 \\ j\omega(C_{0q} + C_{\rm var}) & 1 \end{bmatrix}, \tag{4}$$

where $C_{0q}$ represents the intrinsic capacitance of the line and $C_{\rm var}$ is the average capacitance of the varactors for a given dc bias.

Iteratively multiplying the ray transfer matrix of the $Q$ uniform subsections, considering subsections with shunt varactors, gives the total ray transfer matrix of the continuously spatially varying transmission line. It should be noted that the characteristic impedance function $z_q$ in (4) must satisfy the fabrication condition of $z_{\rm min} < z_q(z) < z_{\rm max}$. Next, the transmission scattering parameter $S_{21}$ of the entire structure may be achieved using the four elements of the ray transfer matrix of the structure, as $S_{21}(\omega) = 2/(A + BZ_0^{-1} + CZ_0 + D)$, where $Z_0$ is the reference characteristic impedance of the load and source. The dispersion relation of the aperiodic nonuniform transmission line will be achieved using the phase angle of the transmission scattering parameter as $\phi_{S_{21}}(\omega)/L$. The characteristic impedances of $q$ uniform subsections in (4), $z_q$, will be computed through achieving the desired passbands and band gaps as

$$|S_{21}(\omega_0,\omega_{\rm p},\omega_1)| = 1, \tag{5a}$$

$$|S_{21}(\omega < \omega_0, \omega_0 < \omega < \omega_{\rm p}, \omega_1 < \omega)| \to 0. \tag{5b}$$

We shall then use the characteristic impedance function $z_{\rm ap}(z;\omega)$ and calculate the corresponding permittivity $\epsilon_{\rm ap}(z;\omega)$, inductance $L_{\rm ap}(z;\omega)$, and capacitance $C_{\rm ap}(z;\omega)$ of the transmission line [50–52], where $z_{\rm ap}(z;\omega) = \sqrt{L_{\rm ap}(z;\omega)/C_{\rm ap}(z;\omega)}$. Then, the permeability of the transmission line may be computed as

$$\mu_{\rm ap}(z;\omega) = \frac{c^2}{\epsilon_{\rm ap}(z;\omega)} L_{\rm ap}(z;\omega) C_{\rm ap}(z;\omega). \tag{6}$$

## IV. ANALYTICAL SOLUTION FOR ELECTROMAGNETIC FIELDS

This section derives a general analytical solution which may be used for aperiodic/periodic space-time modulated media. Inside the modulated medium in Fig. 2, with aperiodic constitutive parameters in (1), the source-less Maxwell equations read

$$\nabla \times \mathbf{E}(z,t;\omega_n) = -\mu(z;\omega)\frac{\partial \mathbf{H}(z,t;\omega_n)}{\partial t}, \tag{7a}$$

$$\nabla \times \mathbf{H}(z,t;\omega_n) = \frac{\partial[\epsilon(z,t;\omega)\mathbf{E}(z,t;\omega_n)]}{\partial t}. \tag{7b}$$

Inserting the electric and magnetic fields in (2) into (7), and following the procedure described in the Supplemental Material [51], we achieve the electric and magnetic coupled mode equations in matrix form as

$$\frac{\partial \mathbf{E}(z;\omega_n)}{\partial z} = \mathbf{Z}(z;\omega_n)\mathbf{H}(z;\omega_n), \tag{8a}$$

$$\frac{\partial \mathbf{H}(z;\omega_n)}{\partial z} = \mathbf{Y}(z;\omega_n)\mathbf{E}(z;\omega_n), \tag{8b}$$

where $\mathbf{E}(z;\omega_n)=[E_{-N}(z;\omega_{-N})\cdots E_0(z;\omega_0)\cdots E_N(z;\omega_N)]^{\rm T}$, $\mathbf{H}(z;\omega_n) = [H_{-N}(z;\omega_{-N})\cdots H_0(z;\omega_0)\cdots H_N(z;\omega_N)]^{\rm T}$, and

$$\mathbf{Z}(z;\omega_n) = i\mu_0\mu_{\rm ap}(z;\omega)\mathbf{W}(\omega_n), \tag{8c}$$

$$\mathbf{Y}(z;\omega_n) = i\epsilon_0\epsilon_{\rm ap}(z;\omega)\mathbf{W}(\omega_n) \times \begin{bmatrix} 1 & \frac{\delta_{\rm p}}{2}e^{-i\beta_{\rm p}z} & 0 & \cdots 0 \\ \frac{\delta_{\rm p}}{2}e^{i\beta_{\rm p}z} & 1 & \frac{\delta_{\rm p}}{2}e^{-i\beta_{\rm p}z} & \cdots 0 \\ 0 & \frac{\delta_{\rm p}}{2}e^{i\beta_{\rm p}z} & 1 & \cdots 0 \\ \vdots & \vdots & \vdots & \ddots \vdots \\ 0 & 0 & 0 & \cdots 1 \end{bmatrix}, \tag{8d}$$

with $\mathbf{W}(\omega_n) = {\rm diag}[\omega_{-N}\cdots\omega_0\cdots\omega_N]$. Two aperiodic functions in (8c) and (8d), i.e., $\mu_{\rm ap}(z;\omega)$ and $\epsilon_{\rm ap}(z;\omega)$, are to be found through the synthesis procedure (Sec. III), satisfying (5). To solve the matrix coupled equation in (8), we first express the desired $\mathbf{Z}(z;\omega_n)$ and $\mathbf{Y}(z;\omega_n)$ functions with $2M+1$ exponential terms as

$$\mathbf{Z}(z;\omega_n) = \sum_{m=-M}^{M} \mathbf{Z}_m(\omega_n)\exp[(im\gamma z)/L], \tag{9a}$$

$$\mathbf{Y}(z;\omega_n) = \sum_{m=-M}^{M} \mathbf{Y}_m(\omega_n)\exp[(im\gamma z)/L], \tag{9b}$$

where $\gamma$ is an unknown rational number between 0 and $2\pi$, and $\mathbf{Z}_m(\omega_n)$ and $\mathbf{Y}_m(\omega_n)$ are unknown coefficient matrices. We next define the electric and magnetic fields as $2M+1$ number of Bloch-like spatial waves as

$$\mathbf{E}(z;\omega_n) = \mathbf{K}(z)\sum_{m=-M}^{M} \mathbf{E}_m(\omega_n)\exp[(im\gamma z)/L], \tag{10a}$$

$$\mathbf{H}(z;\omega_n) = \mathbf{K}(z)\sum_{m=-M}^{M} \mathbf{H}_m(\omega_n)\exp[(im\gamma z)/L]. \tag{10b}$$

In (10a) and (10b), the coefficients $\mathbf{E}_m(\omega_n)$ and $\mathbf{H}_m(\omega_n)$ are unknown electric and magnetic field matrices, and

$$\mathbf{K}(z) = {\rm diag}[\exp(\kappa_{-N}z)\cdots\exp(\kappa_0 z)\cdots\exp(\kappa_N z)] \tag{10c}$$

is the principal spatial frequency matrix. Inserting (9a)–(10c) into the coupled mode equation matrices in (8) yields $2M+1$ set of space-independent matrix equations as

$$\mathbf{E}_m(\omega_n) = \mathbf{\Lambda}_m \sum_{n=-M}^{M} \mathbf{Z}_{m-n}(\omega_n)\mathbf{H}_n(\omega_n), \tag{11a}$$

$$\mathbf{H}_m(\omega_n) = \mathbf{\Lambda}_m \sum_{n=-M}^{M} \mathbf{Y}_{m-n}(\omega_n)\mathbf{E}_n(\omega_n), \tag{11b}$$

where

$$\mathbf{\Lambda}_m = \mathrm{diag}[(\kappa_{-N} + im\gamma/L)^{-1} \cdots (\kappa_N + im\gamma/L)^{-1}], \tag{11c}$$

for $m = -M, \ldots, 0, \ldots, M$. The set of $2M+1$ space-independent coupled mode matrix equations in (11) may be expressed as

$$\overrightarrow{\mathbf{E}}_m(\omega_n) = \overrightarrow{\mathbf{\Lambda}}_m \overrightarrow{\mathbf{Z}}(\omega_n)\overrightarrow{\mathbf{H}}_m(\omega_n), \tag{12a}$$

$$\overrightarrow{\mathbf{H}}_m(\omega_n) = \overrightarrow{\mathbf{\Lambda}}_m \overrightarrow{\mathbf{Y}}(\omega_n)\overrightarrow{\mathbf{E}}_m(\omega_n), \tag{12b}$$

In (12), $\overrightarrow{\mathbf{E}}_m = [\mathbf{E}_{-M} \cdots \mathbf{E}_0 \cdots \mathbf{E}_M]^{\mathrm{T}}$, $\overrightarrow{\mathbf{H}}_m = [\mathbf{H}_{-M} \cdots \mathbf{H}_0 \cdots \mathbf{H}_M]^{\mathrm{T}}$, and

$$\overrightarrow{\mathbf{Z}} = \begin{bmatrix} \mathbf{Z_0} & \mathbf{Z}_{-1} & \cdots & \mathbf{Z}_{-2M+1} & \mathbf{Z}_{-2M} \\ \mathbf{Z}_1 & \mathbf{Z}_0 & \cdots & \mathbf{Z}_{-2M+2} & \mathbf{Z}_{-2M+1} \\ \vdots & \vdots & \ddots & \vdots & \vdots \\ \mathbf{Z}_{2M-1} & \mathbf{Z}_{2M-2} & \cdots & \mathbf{Z}_0 & \mathbf{Z}_{-1} \\ \mathbf{Z}_{2M} & \mathbf{Z}_{2M-1} & \cdots & \mathbf{Z}_1 & \mathbf{Z}_0 \end{bmatrix}, \tag{12c}$$

with

$$\overrightarrow{\mathbf{Y}} = \begin{bmatrix} \mathbf{Y_0} & \mathbf{Y}_{-1} & \cdots & \mathbf{Y}_{-2M+1} & \mathbf{Y}_{-2M} \\ \mathbf{Y}_1 & \mathbf{Y}_0 & \cdots & \mathbf{Y}_{-2M+2} & \mathbf{Y}_{-2M+1} \\ \vdots & \vdots & \ddots & \vdots & \vdots \\ \mathbf{Y}_{2M-1} & \mathbf{Y}_{2M-2} & \cdots & \mathbf{Y}_0 & \mathbf{Y}_{-1} \\ \mathbf{Y}_{2M} & \mathbf{Y}_{2M-1} & \cdots & \mathbf{Y}_1 & \mathbf{Y}_0 \end{bmatrix}, \tag{12d}$$

$$\overrightarrow{\mathbf{\Lambda}}_m = \mathrm{diag}\{[\mathbf{\Lambda}_{-M} \cdots \mathbf{\Lambda}_0 \cdots \mathbf{\Lambda}_M]\}, \tag{12e}$$

$$[\overrightarrow{\mathbf{\Lambda}}_m \overrightarrow{\mathbf{Z}}(\omega_n)\overrightarrow{\mathbf{\Lambda}}_m \overrightarrow{\mathbf{Y}}(\omega_n) - \mathbf{I}]\overrightarrow{\mathbf{E}}(\omega_n) = 0, \tag{13}$$

where $\mathbf{I}$ is a $(2M+1) \times (2M+1)$ identity matrix. The eigenvalue problem in (13) has nontrivial solutions if

$$\det\{[\overrightarrow{\mathbf{\Lambda}}_m \overrightarrow{\mathbf{Z}}(\omega_n)\overrightarrow{\mathbf{\Lambda}}_m \overrightarrow{\mathbf{Y}}(\omega_n) - \mathbf{I}]\} = 0. \tag{14}$$

We shall finally consider the initial conditions at $z = 0$, i.e.,

$$\mathbf{E}(0) = \sum_{m=-M}^{M} \mathbf{E}_m = \mathbf{E}_{\mathrm{i}}, \tag{15}$$

where $\mathbf{E}_{\mathrm{i}} = [0 \cdots 0 E_{\mathrm{i}} 0 \cdots 0]^{\mathrm{T}}$.

## V. EXPERIMENTAL IMPLEMENTATION

This section experimentally demonstrates the application of the aperiodic space-time modulated medium, shown in Figs. 2 and 3, to pure frequency mixing. To best show the effect of the dispersion tailoring in suppression of unwanted space-time harmonics, we compare the experimental results of the proposed spatially aperiodic space-time modulated mixer with those of the conventional periodic uniform space-time modulated medium. The specifications of the mixer are $L = 0.1778$ m, $\omega_0 = 2\pi \times 300$ MHz, $\omega_{\mathrm{p}} = 2\pi \times 700$ MHz, and $\omega_1 = 2\pi \times 1000$ MHz. Figure 4(a) plots the *tailored* aperiodic spatial variation of the permittivity of the mixer, optimized using the synthesis method in Sec. III, and compared with the results of the series expansion in (9a) for $\gamma = 5.677$ and $M = 30$. Figure 4(b) plots the *tailored* aperiodic spatial variation of the permeability of the mixer, optimized using the synthesis method in Sec. III, compared with the results of the series expansion in (9b) for $\gamma = 5.677$ and $M = 30$.

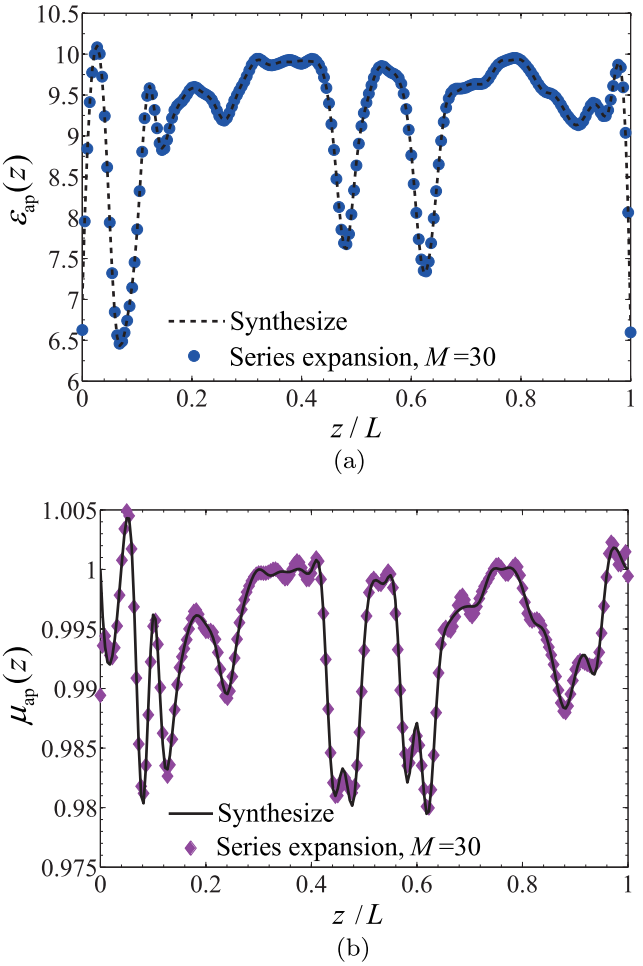


FIG. 4. Aperiodic spatial variation of the constitutive parameters of the mixer in Fig. 3, achieved using the synthesis method in Sec. III, and compared with the analytical results, using the series expansion in (9a) and (9b), for $\gamma = 5.677$ and $M = 30$. (a) Permittivity $\epsilon_{\mathrm{ap}}(z)$. (b) Permeability $\mu_{\mathrm{ap}}(z)$.

Figure 5(a) plots the analytical results for the dispersion diagram of the dominant mode, i.e., $\mathrm{Re}\{\beta(\omega)\}$, for the unbounded aperiodic dispersion-tailored space-time modulated mixer with the optimized permittivity and permeability in (1). It may be seen from this figure that such a dispersion-tailored structure provides large and aperiodic band gaps at desired

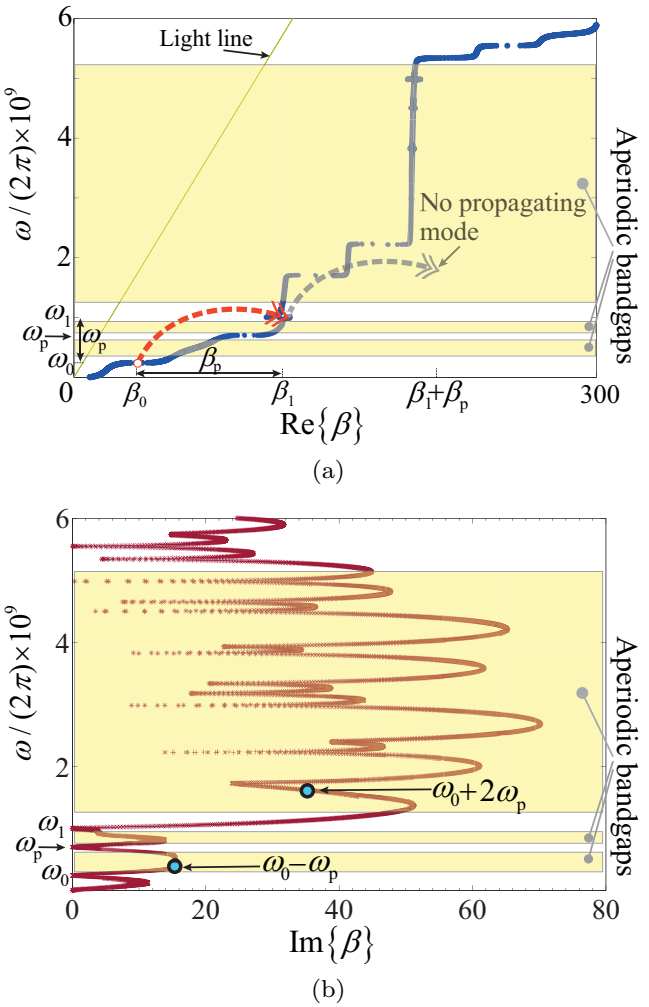


FIG. 5. Analytical results for the dispersion of the aperiodic space-time modulated waveguide in Fig. 3. (a) Real part of the wave number, where aperiodic photonic band gaps prohibit harmonic transitions to undesirable space-time harmonics. Three passbands are considered for the propagation of input and output waves at $\omega_0$, $\omega_p$, and $\omega_1$. (b) Imaginary part of the wave number, where the suppression of the first undesirable harmonics at $\omega_0 + 2\omega_p$ is highlighted with a circle.

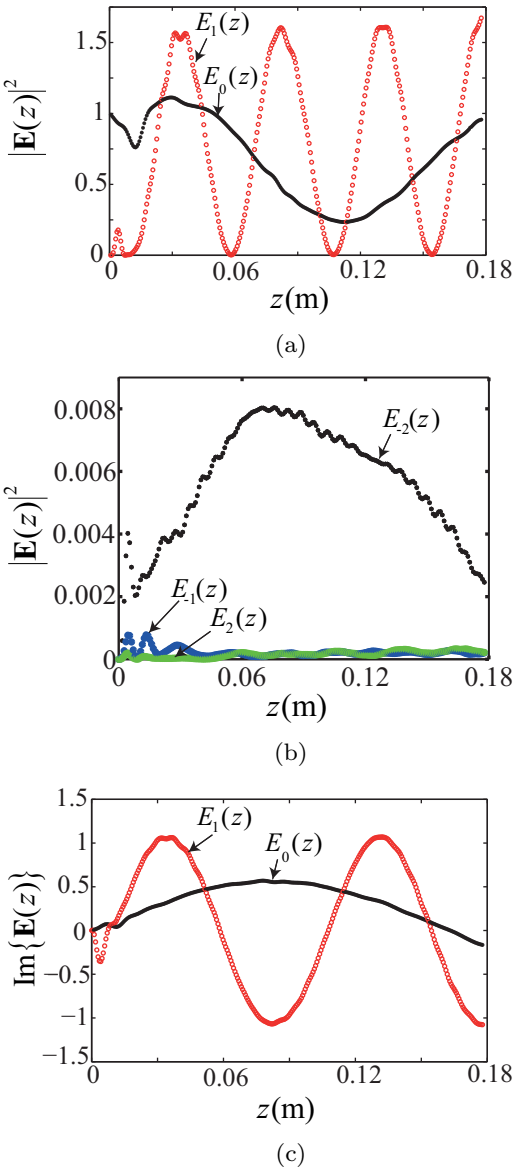


FIG. 6. Analytical results for the electric field inside the space-time modulated mixer with aperiodic spatially variant constitutive parameters in Fig. 4, and using (10a). (a) Time-averaged magnitude of the pointing vectors of the input wave at $\omega_0$ and the fundamental harmonic at $\omega_1$, multiplied by $2\sqrt{\mu_0/\epsilon_0}$, i.e., $|E_0(z)|^2$ and $|E_1(z)|^2$. (b) Time-averaged magnitude of the pointing vectors of higher-order harmonics at $-\omega_0+\omega_p$, $-\omega_0+2\omega_p$, and $\omega_0+2\omega_p$, multiplied by $2\sqrt{\mu_0/\epsilon_0}$, i.e., $|E_{-2}(z)|^2$, $|E_{-1}(z)|^2$, and $|E_2(z)|^2$. (c) Imaginary part of the electric fields at $\omega_0$ and $\omega_1$, $\mathrm{Im}\{E_0(z)\}$ and $\mathrm{Im}\{E_1(z)\}$.

frequency bands, prohibiting transition to the undesired space-time harmonics. It should be noted that, since the structure is time periodic, time harmonics occur at $\omega_0 + n\omega_p$. However, thanks to the tailored spatial aperiodicity of the structure, except $\omega_0$ and $\omega_1$, all the time harmonics lie in the band gap of the structure and hence will not grow up, but rather propagate as weak waves and are attenuated. Figure 5(b) plots the corresponding analytical results for the imaginary part of the wave number of the dominant mode, i.e., $\mathrm{Im}\{\beta(\omega)\}$. This figure exhibits the suppression level at different band gaps for undesired harmonics. It should be noted that, except for the input wave at $\omega_0$, the power level of all the space-time harmonics is equal to zero at the input of the structure, i.e., at $z = 0$. As a result, the band gaps are to prohibit growth of the power of the undesired harmonics, rather than attenuation of the strong waves. Consequently, even a weak or moderate attenuation in a band gap may lead to strong suppression of the corresponding space-time harmonic.

Figure 6(a) plots the analytical results for the time-averaged magnitude of the pointing vectors of two main harmonics multiplied by $2\sqrt{\mu_0/\epsilon_0}$, i.e., $|E_0(z)|^2$ and $|E_1(z)|^2$. At $z = 0$, the amplitude of the input wave $\omega_0$ and the first harmonic $\omega_1$ are respectively equal to the unity and zero. As the input wave propagates through the structure, progressive transition of the energy and momentum occurs to the desired space-time harmonic at $\omega_1$. Figure 6(b) plots the analytical results for

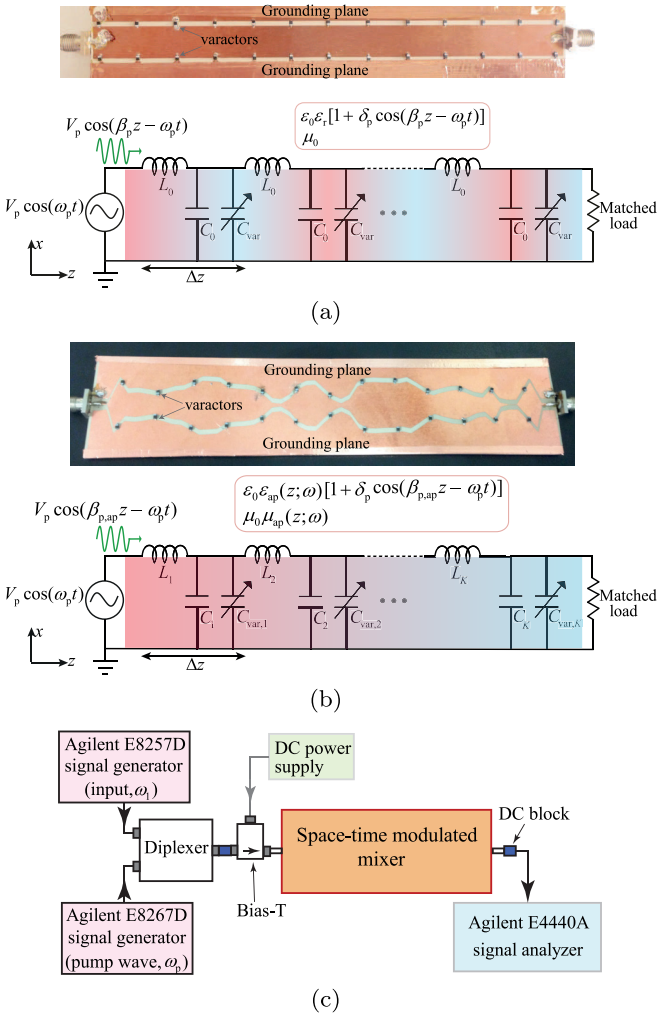


FIG. 7. Experimental demonstration of space-time modulated mixers. (a) An image and the equivalent circuit model of the fabricated periodic space-time modulated mixer using an array of varactors distributed on top of a periodic uniform coplanar waveguide. (b) An image and the equivalent circuit model of the fabricated aperiodic dispersion-tailored space-time modulated mixer using an array of varactors distributed on top of an aperiodic spatially varying coplanar waveguide. (c) Measurement setup.

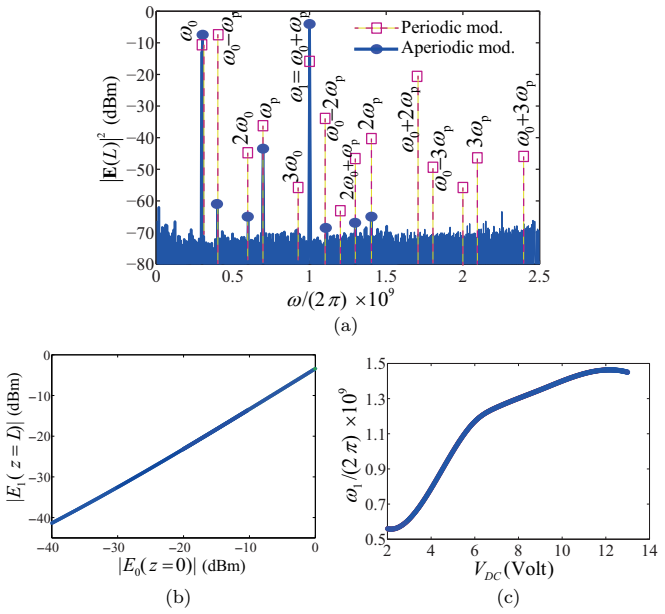


FIG. 8. Experimental results. (a) Comparison of the output spectra of the periodic and aperiodic space-time modulated structures, respectively, in Figs. 7(a) and 7(b). The space-time harmonics occur at $|k\omega_0 + n\omega_p|$, where for the dispersion-tailored aperiodic space-time modulated mixer, the power level of the unwanted harmonics is negligible. (b) The ratio between the amplitude of the output and input waves of the aperiodic dispersion-tailored space-time modulated mixer in Fig. 7(b), $|E_1|/|E_0|$, revealing a linear response of the system. (c) Tuning the output frequency of the mixer $\omega_1$ (and the corresponding $\omega_m$) using the average capacitance of varactors through their average dc voltage.

the time-averaged magnitude of the pointing vectors of the higher-order undesired harmonics multiplied by $2\sqrt{\mu_0/\epsilon_0}$, i.e., $|E_{-2}(z)|^2$, $|E_{-1}(z)|^2$, and $|E_2(z)|^2$. At $z = 0$, the amplitude of all these space-time harmonics, $\omega_{-2}$, $\omega_{-1}$, and $\omega_2$, is equal to zero. Since the structure is time periodic, all the harmonics are physically generated and are nonzero. However, as they lie in the band gap of the structure, they will not progressively grow up through the structure, but rather propagate as weak waves and are suppressed. Figure 6(b) plots the analytical results for the imaginary part of the electric fields of the fundamental and first harmonic, $\mathrm{Im}\{E_0(z)\}$ and $\mathrm{Im}\{E_1(z)\}$.

Figure 7(a) shows an image of the fabricated periodic space-time modulated medium and its equivalent circuit model. The structure is realized using an array of varactors subwavelength distributed on top of a uniform conductor-backed coplanar waveguide with the dispersion diagram in Fig. 1(a), where photonic transition from the fundamental harmonic $\omega_0$ to all space-time harmonics are allowed. In the circuit model, $L_0$ and $C_0$ respectively represent the intrinsic inductance and capacitance of the transmission line, and $C_{\mathrm{var}}$ denotes the variable capacitance. The array of varactors is spatiotemporally modulated using a harmonic generator, with the amplitude $V_p \cos(\omega_p t)$, propagating in the $+z$ direction.

Figure 7(b) shows an image of the fabricated dispersion-tailored spatially aperiodic space-time modulated mixer and the corresponding equivalent circuit model. In this scheme, an array of subwavelength spaced varactors is placed on top of an aperiodic spatially varying conductor-backed coplanar waveguide. It may be seen in the circuit model that all the intrinsic inductance, intrinsic capacitance, and variable capacitance of the structure are varying in space, where the structure is space-time modulated using the same harmonic generator as in Fig. 7(a). Figure 7(c) illustrates the measurement setup composed of the feeding network and a signal analyzer. The feeding network includes a diplexer which combines the input wave at $\omega_1$ and the pump wave at $\omega_p$, provided by two signal generators, and a bias $T$ superimposing the dc bias.

Figure 8(a) compares the experimental results of the output spectra of the periodic and aperiodic space-time modulated frequency mixers, shown respectively in Figs. 7(a) and 7(b). It may be seen from this figure that the periodic space-time modulated mixer provides all, undesirable space-time harmonics at its output, i.e., $|k\omega_0 + n\omega_p|$, where the strongest transition

occurs from $\omega_0$ to the unwanted harmonic at $|\omega_0 - \omega_p|$. This is due to the fact that the varactors are dispersive and exhibit their highest efficiency at low frequencies. In contrast, the aperiodic dispersion-tailored space-time modulated mixer, shown in Fig. 7(b), provides the required energy and momentum for a pure transition from the input frequency $\omega_0$ to the desirable harmonic at $\omega_0 + \omega_p$ and prohibits transition to undesirable harmonics. Figure 8(b) investigates the linear response of the aperiodic dispersion-tailored space-time modulated mixer in Fig. 7(b). This figure demonstrates that the output of the structure linearly follows the input, i.e., $|E_1|/|E_0| = \text{const}$. The linear property of the space-time modulated medium may also be seen in (15), where the amplitude of the space-time harmonics linearly follows the input wave. It should be noted that changing the applied dc bias of varactors will alter the average permittivity $\epsilon_{ap}$ of the structure, dispersion diagram (band gaps), and the space-time pumping depth $\delta_p$. As a result, the pump and output frequencies may be tuned via the applied dc bias. Figure 8(c) plots the variation of the output frequency $\omega_1$ versus the applied dc bias of varactors. Therefore, the operation frequencies of this mixer may be tuned.

Such pure frequency mixer provides an important step toward integrated broadband and high isolation microwave and optical mixing technologies. Moreover, it may present conversion gain for greater pumping depths. The ratio $|E_1|/|E_0|$ at the output of the mixer can be further enhanced using appropriate design and fabrication of the coplanar waveguide and lumped elements. Appropriate structures may be envisioned at terahertz and optics, for instance, using dielectric slabs doped to create *p-i-n* junction schemes responding to a pump wave and operate as voltage-tunable capacitors [16,53].

## VI. CONCLUSIONS

This study investigated the effects of inharmonic and distinct photonic transition in an aperiodic space-time modulated medium. Leveraging peculiar properties of tailored aperiodic space-time modulation, we presented a pure frequency mixer. In contrast to periodic space-time modulated media and conventional mixers, the proposed mixer is immune to undesirable mixing products. A rigorous analytical solution is provided for the electromagnetic field solution inside general aperiodic/periodic space-time modulated media. The experimental demonstration of this mixer is provided using an array of subwavelength-spaced space-time modulated varactors mounted on top of an aperiodic spatially variant coplanar waveguide. Aperiodic space-time modulated medium is endowed with aperiodic photonic band gaps which may be utilized for various wave transformations. It is expected to find a range of complementary applications, such as, for instance, in metasurface technology, illusion cloaks, subharmonic frequency mixing, nonreciprocal structures, and optical frequency generators.


[1] S. A. Maas, *Microwave Mixers*, 2nd ed. (Artech House, Norwood, Massachusetts, 1993).

[2] B. Henderson and E. Camargo, *Microwave Mixer Technology and Applications* (Artech House, Norwood, Massachusetts, 2013).

[3] J. Hashimoto, K. Itoh, M. Shimozawa, and K. Mizuno, Fundamental limitations on the output power and the third-order distortion of balanced mixers and even harmonic mixers, IEEE Trans. Microwave Theory Tech. **64**, 2853 (2016).

[4] T. Vasseaux, B. Huyart, P. Loumeau, and J. Naviner, A track and hold-mixer for direct-conversion by subsampling, *Proceedings of the IEEE International Symposium on Circuits and Systems* (IEEE, Piscataway, NJ, 1999).

[5] H. Pekau and J. W. Haslett, A 2.4 GHz CMOS sub-sampling mixer with integrated filtering, IEEE J. Solid-State Circ. **40**, 2159 (2005).

[6] T. Jiang, R. Wu, S. Yu, D. Wang, and W. Gu, Microwave photonic phase-tunable mixer, Opt. Express, **25**, 4519 (2017).

[7] A. L. Cullen, A travelling-wave parametric amplifier, Nature (London) **181**, 332 (1958).

[8] E. S. Cassedy and A. A. Oliner, Dispersion relations in time-space periodic media: Part I—Stable interactions, Proc. IEEE **51**, 1342 (1963).

[9] J. N. Winn, S. Fan, J. D. Joannopoulos, and E. P. Ippen, Interband transitions in photonic crystals, Phys. Rev. B **59**, 1551 (1999).

[10] Z. Yu and S. Fan, Complete optical isolation created by indirect interband photonic transitions, Nat. Photonics **3**, 91 (2009).

[11] S. Taravati, N. Chamanara, and C. Caloz, Nonreciprocal electromagnetic scattering from a periodically space-time modulated slab and application to a quasisonic isolator, Phys. Rev. B **96**, 165144 (2017).

[12] N. Chamanara, Z.-L. Deck-Léger, C. Caloz, and D. Kalluri, New electromagnetic modes in space-time modulated dispersion-engineered media, arXiv:1710.01625.

[13] S. Taravati, Application of space- and time-modulated dispersion engineered metamaterials to signal processing and magnetless nonreciprocity, Ph.D. thesis, École Polytechnique de Montréal, 2017.

[14] X. Huang and S. Fan, Complete all-optical silica fiber isolator via stimulated Brillouin scattering, J. Lightwave Technol. **29**, 2267 (2011).

[15] M. S. Kang, A. Butsch, and P. S. J. Russell, Reconfigurable light-driven opto-acoustic isolators in photonic crystal fibre, Nat. Photonics **5**, 549 (2011).

[16] H. Lira, Z. Yu, S. Fan, and M. Lipson, Electrically Driven Nonreciprocity Induced by Interband Photonic Transition on a Silicon Chip, Phys. Rev. Lett. **109**, 033901 (2012).

[17] C. G. Poulton, R. Pant, A. Byrnes, S. Fan, M. J. Steel, and B. J. Eggleton, Design for broadband on-chip isolator using stimulated Brillouin scattering in dispersion-engineered chalcogenide waveguides, Opt. Express **20**, 21235 (2012).

[18] N. Chamanara, S. Taravati, Z.-L. Deck-Léger, and C. Caloz, Electromagnetic nonreciprocity and perfect mixing in space-time engineered asymmetric bandgaps, *Proceedings of the IEEE AP-S Int. Antennas Propagat. (APS)* (IEEE, Piscataway, NJ, 2017).

[19] S. Taravati, Self-biased broadband magnet-free linear isolator based on one-way space-time coherency, Phys. Rev. B **96**, 235150 (2017).

[20] N. A. Estep, D. L. Sounas, J. Soric, and A. Alù, Magnetic-free non-reciprocity and isolation based on parametrically modulated coupled-resonator loops, Nat. Photonics **10**, 923 (2014).

[21] T. Dinc, M. Tymchenko, A. Nagulu, D. Sounas, A. Alù, and H. Krishnaswamy, Synchronized conductivity modulation to realize broadband lossless magnetic-free non-reciprocity, Nat. Commun. **8**, 795 (2017).

[22] Y. Hadad, D. L. Sounas, and A. Alù, Space-time gradient metasurfaces, Phys. Rev. B **92**, 100304 (2015).

[23] A. Shaltout, A. Kildishev, and V. Shalaev, Time-varying metasurfaces and Lorentz nonreciprocity, Opt. Mater. Express **5**, 2459 (2015).

[24] Y. Shi and S. Fan, Dynamic non-reciprocal meta-surfaces with arbitrary phase reconfigurability based on photonic transition in meta-atoms, Appl. Phys. Lett. **108**, 021110 (2016).

[25] Y. Shi, S. Han, and S. Fan, Optical circulation and isolation based on indirect photonic transitions of guided resonance modes, ACS Photonics **4**, 1639 (2017).

[26] S. Taravati and C. Caloz, Space-time modulated nonreciprocal mixing, amplifying and scanning leaky-wave antenna system, *Proceedings of the IEEE AP-S Int. Antennas Propagat. (APS)* (IEEE, Piscataway, NJ, 2015).

[27] Y. Hadad, J. C. Soric, and A. Alù, Breaking temporal symmetries for emission and absorption, Proc. Natl. Acad. Sci. USA **113**, 3471 (2016).

[28] S. Taravati and C. Caloz, Mixer-duplexer-antenna leaky-wave system based on periodic space-time modulation, IEEE Trans. Antennas Propag. **65**, 442 (2017).

[29] S. Y. Elnaggar and G. N. Milford, Controlling non-reciprocity using enhanced Brillouin scattering, arXiv:1707.00050.

[30] G. M. Roe and M. R. Boyd, Parametric energy conversion in distributed systems, Proc. IRE **47**, 1213 (1959).

[31] Y. Hadad, J. Soric, and A. Alù, Spatiotemporally modulated antennas, *Proceedings of the CNC/USNC URSI National Radio Science Meeting* (IEEE, Piscataway, NJ, 2015), p. 159.

[32] S. Taravati and M. Khalaj-Amirhosseini, Generalised single-section broad-band asymmetrical Wilkinson power divider, IET Microw. Antennas Propagat. **6**, 1164 (2012).

[33] S. Taravati and M. Khalaj-Amirhosseini, An efficient method of designing dual- and wide-band power dividers with arbitrary power division, Int. J. RF Microw. Comput. Aided Eng. **23**, 118 (2013).

[34] T. Dhaene, L. Martens, and D. D. Zutter, Transient simulation of arbitrary nonuniform inetrconnection structures characterized by scattering parameters, IEEE Trans. Circuit Syst. **39**, 928 (1992).

[35] J. E. Schutt-Aine, Transient analysis of nonuniform transmission lines, IEEE Trans. Circuit Syst. **39**, 378 (1992).

[36] S. Taravati and M. Khalaj-Amirhosseini, Design method for matching circuits of general multiplexers, IET Microw. Antennas Propagat. **7**, 237 (2013).

[37] A. V. Beljaev, A. P. Krenitskiy, V. P. Meschanov, and L. V. Shikova, Directional filters on coupled nonuniform TEM transmission lines, IEEE Trans. Microwave Theory Tech. **52**, 133 (2004).

[38] A. Lujambio, I. Arnedo, M. Chudzik, I. Arregui, T. Lopetegi, and M. A. G. Laso, Dispersive delay line with effective transmission-type operation in coupled-line technology, IEEE Microw. Wireless Compon. Lett. **21**, 459 (2011).

[39] S. Taravati, Q. Zhang, and C. Caloz, Non-uniform C-section phasers for enhanced design flexibility in radio analog signal processing, *Proceedings of the IEEE European Microwave Conference (EuMC)* (IEEE, Piscataway, NJ, 2014).

[40] S. Taravati, S. Gupta, Q. Zhang, and C. Caloz, Enhanced bandwidth and diversity in real-time analog signal processing (R-ASP) using nonuniform C-section phasers, IEEE Microw. Wireless Compon. Lett. **26**, 663 (2016).

[41] S. Taravati and C. Caloz, Versatile phasers constituted of coupling-free nonuniform stub-loaded transmission lines, *Proceedings of the IEEE European Microwave Conference (EuMC)* (IEEE, Piscataway, NJ, 2015).

[42] M. Khalaj-Amirhosseini, Wideband or multiband complex impedance matching using microstrip nonuniform transmission lines, Prog. Electromagn. Res. **66**, 15 (2006).

[43] S. Taravati, Realization of compact broadband rat-race coupler, J. Electromagn. Waves. Appl. **26**, 1708 (2012).

[44] S. Taravati and M. Khalaj-Amirhosseini, Compact dual-band stubless branch-line coupler, J. Electromagn. Waves. Appl. **26**, 1323 (2012).

[45] S. Taravati, Miniaturized wide band rat race coupler, Int. J. RF Microw. Comput. Aided Eng. **23**, 675 (2013).

[46] E. Yablonovitch, Photonic band-gap structures, J. Opt. Soc. Am. B **10**, 283 (1993).

[47] A. A. Oliner, Periodic structures and photonic-band-gap terminology: Historical perspectives, *Proceedings of the IEEE European Microwave Conference (EuMC)* (IEEE, Piscataway, NJ, 1999).

[48] L. Moretti and V. Mocella, Two-dimensional photonic aperiodic crystals based on Thue-Morse sequence, Opt. Express **15**, 15314 (2007).

[49] S. V. Boriskina, A. Gopinath, and L. D. Negro, Optical gaps, mode patterns and dipole radiation in two-dimensional aperiodic photonic structures, Physica E: Low-dimensional Systems and Nanostructures **41**, 1102 (2009).

[50] R. N. Simons, *Coplanar Waveguide Circuits, Components, and Systems* (Wiley, New York, 2001).

[51] See Supplemental Material at http://link.aps.org/supplemental/10.1103/PhysRevB.97.115131 for detailed derivations.

[52] D. M. Pozar, *Microwave Engineering*, 4th ed. (Wiley, New York, 2012).

[53] A. Khilo, C. M. Sorace, and F. X. Kärtner, Broadband linearized silicon modulator, Opt. Express **19**, 4485 (2011).